A Spherical Nucleic Acid Platform Based on Self-Assembled DNA Biopolymer for High-Performance Cancer Therapy

Jing Zheng,[†,‡] Guizhi Zhu,[‡] Yinhui Li,[†] Chunmei Li,[‡,§] Mingxu You,[‡] Tao Chen,[‡] Erqun Song,[‡,§] Ronghua Yang,[†,*] and Weihong Tan[†,‡,*]

[†]Molecular Science and Biomedicine Laboratory, State Key Laboratory of Chemo/Bio-Sensing and Chemometrics, College of Biology, College of Chemistry and Chemical Engineering, Collaborative Innovation Center for Chemistry and Molecular Medicine, Hunan University, Changsha 410082, People's Republic of China, [‡]Center for Research at Bio/nano Interface, Department of Chemistry and Department of Physiology and Functional Genomics, Shands Cancer Center, UF Genetics Institute and McKnight Brain Institute, University of Florida, Gainesville, Florida 32604, United States, and [§]Ministry of Education Key Laboratory on Luminescence and Real-Time Analysis, College of Chemistry and Chemical Engineering, College of Pharmaceutical Science, Southwest University, Chongqing 400715, People's Republic of China

ABSTRACT

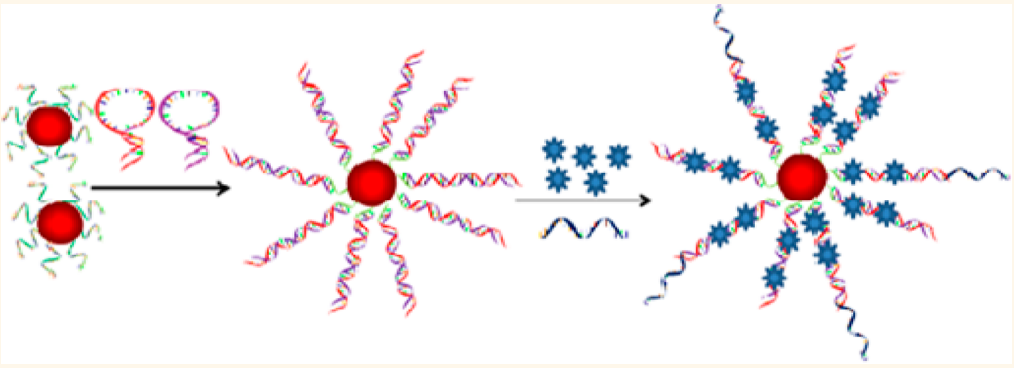

Based on their enhanced cellular uptake, stability, biocompatibility, and versatile surface functionalization, spherical nucleic acids (SNAs) have become a potentially useful platform in biological applications. It still remains important to expand the SNAs' "toolbox", especially given the current interest in multimodal or theranostic nanomaterials, that is, composites capable of multiple simultaneous applications such as imaging, sensing, and drug delivery. In this paper, we have engineered a nanoparticle-conjugated initiator that triggers a cascade of hybridization reactions resulting in the formation of a long DNA polymer as the nanoparticle shell. By employing different DNA fragments, self-assembled multifunctional SNAs can be constructed. Therefore, using one capped ligand, these SNAs can combine imaging fluorescent tags, target recognition element, and targeted delivery molecules together. Since these SNAs possess high drug loading capacity and high specificity by the incorporation of an aptamer, our approach might find potential applications in new drug development, existing drug improvement, and drug delivery for cancer therapy.

KEYWORDS: spherical nucleic acids · DNA hybridization reaction · DNA polymer · drug delivery · cancer therapy

Molecular self-assembly offers a "bottom-up" route to fabricate complex structures from simple components with subnanometer precision. DNA is a promising material for nucleic acid self-assembled structures exhibiting nanoscale dimensions, as reflected by a 3.4 nm length for a complete 10 base helical turn and a diameter corresponding to 2 nm for the duplex DNA.[1,2] The base sequence in DNA encodes considerable structural and functional information into the nanostructure. Based on specific base-pair formation and programmable sequence, DNA nanostructure assembly, pioneered by Seeman *et al.* in the 1980s,[3] has now reached the stage of facile fabrication of complicated 2D and even 3D nanostructures *via* designed hybridization processes. Efforts have been made in both directed assembly of highly complex nanostructures and applications of these

* Address correspondence to tan@chem.ufl.edu, yangrh@pku.edu.cn.

Received for review November 15, 2012 and accepted July 10, 2013.

Published online July 10, 2013
10.1021/nn402344v

nanostructures in molecular sensing,[4,5] nanomachines,[6−8] and drug delivery.[9,10]

The current trend in the fields of life science and biotechnology has been the integration of nanotechnology with biology and chemistry to develop new bioanalytical tools. Nanomaterials, such as metallic nanoparticles, semiconductor nanocrystals, and carbon nanomaterials, have all shown promise as drug and gene delivery vehicles, as well as diagnostic agents. Pioneered by the seminal work of Mirkin *et al.*[11] as early as 1996, polyvalent nucleic acid−nanoparticle conjugates in the form of spherical nanostructures with densely functionalized and highly oriented nucleic acids have been synthesized by covalently attaching the nucleic acid to the gold nanoparticles' surfaces.[11] These well-characterized spherical nucleic acids (SNAs) with gold cores and nucleic acid shells exhibit features that are different from those of nanoparticles and DNA and have catalyzed worldwide interest as novel labels for *in vitro* biodetection,[12−14] intracellular assays,[15,16] as well as potent cell transfection,[17,18] therapeutic,[19] and gene regulation materials.[18,20−22] Recently, to improve drug solubility and delivery efficiency, the drug molecule paclitaxel was covalently labeled to SNAs *via* DNA linkers.[23] The paclitaxel-containing conjugates exhibited >50-fold increase in the solubility over the free paclitaxel, and thus high drug efficacy in paclitaxel-resistant cell lines. However, limitations, such as tedious and intricate synthetic processes for covalent labeling of the drug molecule and insufficient drug payload capacity, still exist and could hamper the transition to practical applications.

To achieve a high-performance SNA-based drug delivery system for cancer therapy, in this paper, we engineered a nanoparticle-conjugated initiator that triggered a cascade of hybridization reactions resulting in the formation of a long DNA polymer as the nanoparticle shell. Then, by employing different DNA fragments, self-assembled multifunctional SNAs were constructed. Compared with traditional SNAs, this strategy possesses several advantages in cancer therapy. First, controllable size of SNAs can be realized by adjusting the concentration of the DNA initiator strand in the DNA-assisted cascade hybridization reaction, which has the potential to control cellular uptake, stability, biocompatibility, and surface functionalization.[24,25] Second, imaging fluorescent tags, target recognition element, and targeted delivery molecules can all be assembled together on the surface of the nanoparticle by one capping ligand. Third, the approach is generalizable because various recognition elements and anticancer drugs can be loaded in this self-assembled DNA biopolymer. As a proof of concept, gold nanoparticles (AuNPs) are initially chosen as the model core materials for investigation of the formation of AuNP-SNAs with controllable size. Then, super-paramagnetic magnetic nanoparticles (MNPs), due to their suitability as theranostic agents, their intrinsic properties endow them with diagnostic capabilities in magnetic resonance imaging (MRI) applications, and their surface can be easily modified by conjugation with various targeting ligands, dyes, and drugs to provide multimodal functionality.[26] Therefore, in the further application, such as cancer therapy in our study, MNPs are then employed to serve as the scaffold of the MNP-SNAs. Meanwhile, aptamers such as AS1411 and Sgc8 are embedded in, or capped on, the assembled biopolymer to endow it with high specific recognition capability. Simultaneous fluorescent imaging can also be achieved by appropriate positioning of multiple chromophores in the self-assembled biopolymer. This new multifunctional SNA platform is expected to be a promising approach for the intracellular quantification of other small molecules or proteins, as well as drug delivery for cancer therapy.

RESULTS AND DISCUSSION

Preparation of AuNP-SNAs. The self-assembled DNA biopolymer on the surface of the nanoparticle is shown in Scheme 1. Hybridization chain reaction (HCR) is where two stable species of DNA hairpins coexist in solution and a single DNA strand initiates the cascade of hybridization to form a long concatamer structure.[27] Each copy of the initiator can propagate a chain reaction of hybridization events between alternating monomer 1 (M1) and monomer 2 (M2) single strands to form a nicked double helix. The citrate-capped AuNPs were first treated with diethyl pyrocarbonate followed by autoclaving treatment functionalized with 3′-alkylthiol-modified initiator using literature procedures.[28] UV−visible spectroscopic measurement was performed to monitor the change of the nanoparticle solution (Figure S1 in the Supporting Information). Because different concentrations of initiator triggered various lengths of DNA biopolymer during the process of HCR, size-controllable AuNP-SNAs could be constructed using different concentrations of initiator after addition of a fixed concentration of M1 and M2. As shown in Figure 1, for M1 and M2 (the concentrations are 400 nM), size-controllable AuNP-SNAs could be attained. As the concentration of initiator conjugated on the surface of AuNPs changed (from 0 to about 100 nM), the hydrodynamic size of AuNP-SNAs characterized by dynamic light scattering (DLS) became larger and larger (from 19.0 ± 1.2 to 130.4 ± 6.8 nm). It was resulted from the low concentration of initiator that can trigger only a small proportion chain reaction of alternating kinetic escapes by the two hairpin species (M1 and M2) corresponding to "polymerization" into a nicked double helix. The length of the self-assembled DNA biopolymer increased as a function of the concentrations of conjugated initiator. However, when the initiator increased to about 100 nM, or even higher,

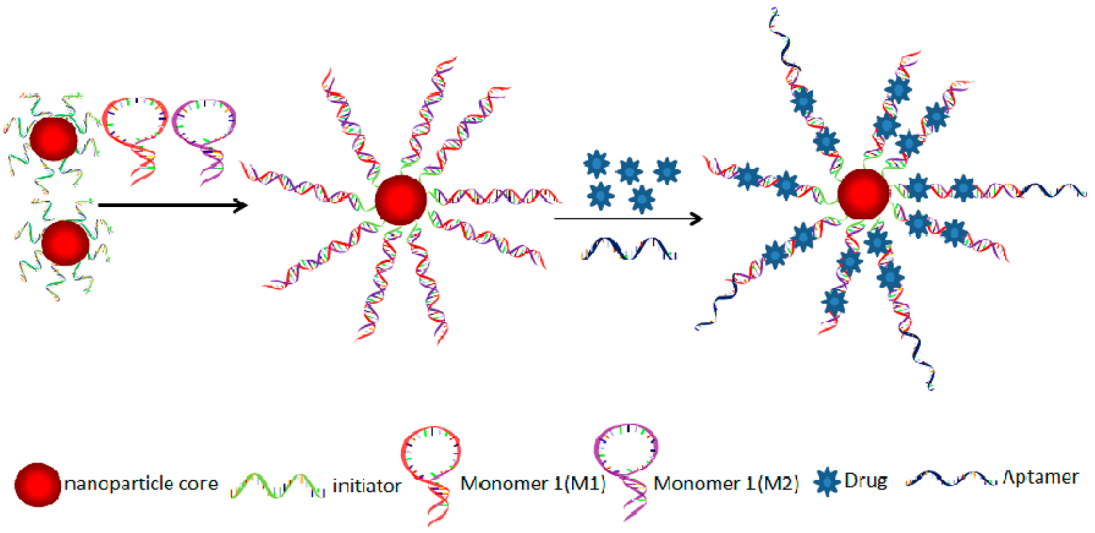

Scheme 1. Schematic representation of multifunctional SNA platform for cancer therapy.

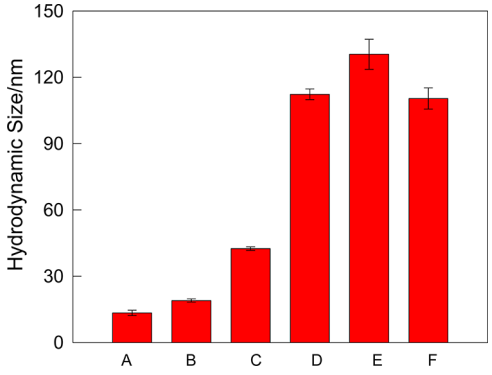

Figure 1. Average hydrodynamic sizes of AuNP-SNAs characterized by DLS. Samples A−F: Concentrations of M1 and M2 were both 400 nM, and the concentration of initiator strand was 0, 9.6 ± 1.2, 18.9 ± 0.8, 40.8 ± 1.3, 78.4 ± 3.4, and 97.6 ± 4.2 nM, respectively.

one should also note that the size of AuNP-SNAs remained fairly constant because the HCR system would finally reach the equilibrium state in terms of kinetics and thermodynamics (the representative size distributions characterized by DLS are shown in Figure S2). Figure S3 shows representative atomic force microscopy (AFM) images of AuNP-SNAs corresponding to various concentrations of conjugated initiators (0 and 97.6 ± 4.2 nM), confirming that the size increase was due to DNA assembly and not nanoparticle aggregation. The AFM results indicated that, for a high concentration of conjugated initiator (97.6 ± 4.2 nM), the mean diameter of nanoparticles was roughly 70 nm. In general, the results often show differences for size measurements between AFM and DLS, and the latter was mainly a result from hydrodynamic size in solution, which is much larger.[29] In addition, the concentrations of self-assembled M1 and M2 for each size of AuNP-SNAs are summarized in Table S2. Figure S4 further shows the agarose gel electrophoresis image of one specific length of DNA biopolymer self-assembled on the surface of AuNPs at a size of 130.5 ± 6.8 nm. After treatment with 10 mM DTT to destroy the Au−S bond, the supernatant solution was collected, and the result also confirmed that the formation of initiator DNA had actually assisted the self-assembled concatamer structure.

Construction of AS1411/MNP-SNAs. As a further application of this concept, the aptamer sequence AS1411 specific to cancer cells with high expression of nucleolin was chosen as the model targeted cell recognition element embedded in the self-assembled DNA biopolymer. The 26-mer guanine-rich aptamer AS1411(5′-GGTGGTGGTGGTTGTGGTGGTGGTGG-3′) has been in phase II clinical trials for relapsed or refractory acute myeloid leukemia and for renal cell carcinoma.[30] When AS1411 forms a stable G-quadruplex structure, it shows high binding affinity to nucleolin, which is overexpressed in tumor cells. Aptamer AS1411 characterized by the G-quadruplex structure was a stable candidate for carrying a quadruplex ligand, such as 5,10,15,20-tetrakis(4-*N*-methylpyridiniumyl)porphyrin (TMPyP4). TMPyP4 is a broadly used photodynamic therapy (PDT) reagent which has been identified as an effective G-quadruplex DNA-binding ligand.[31−35] However, TMPyP4 has poor selectivity and is toxic to some normal cell lines, especially normal fibroblasts and epithelium, when exposed to light.[33] Therefore, in recent studies, targeted delivery, such as aptamer, has been successfully used to increase the accumulation at the target site and to prevent toxicity to the neighboring tissues.[36,37] Compared to this reported work, a new AS1411/MNP-SNA platform was proposed in our design, and multiple copies of AS1411 could be embedded in the long DNA biopolymer on the surface of the nanoparticle. Meanwhile, simultaneous fluorescent imaging could also be realized by appropriate positioning of multiple chromophores; therefore, high drug loading efficacy, high specific binding, and

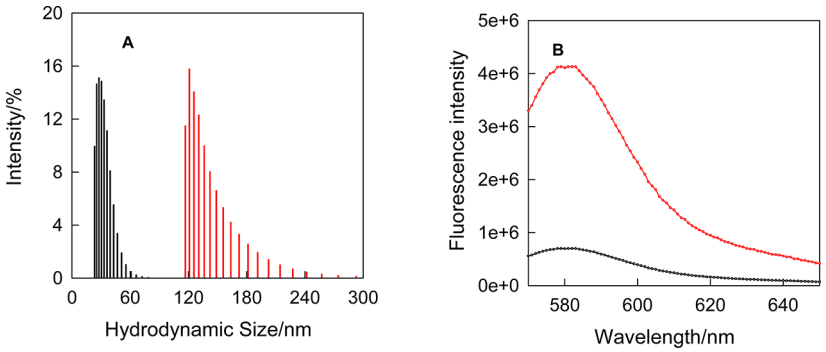

Figure 2. (A) Hydrodynamic size distribution characterized by DLS and (B) fluorescent spectrum of biotin-M3-TAMRA directly conjugated MNPs (black) and TAMRA-labeled AS1411/MNP-SNAs (red), with excitation at 560 nm. The concentration of MNPs is 5 nM.

multifunctional application can be achieved. For the construction of AS1411/MNP-SNAs, another series of monomer sequences besides M2 containing AS1411 at different positions were employed initially (M3 and M4; see sequences in Table S1). The formation of the AS1411 biopolymer was compared by agarose gel electrophoresis images (Figure S5). The slow migration band corresponded to the longer polymer during the HCR because of high molecular weight. Therefore, comparing all the bands in the image, we concluded that M2 and M3 were the optimal monomer probes for subsequent studies and the superior molar ratio of initiator, M2, and M3 is 2:10:10 to get the highest efficiency of HCR. As shown in Figure 2A, DLS results demonstrated that the biotin-initiator-conjugated streptavidin-coated MNPs had an average hydrodynamic diameter (d) of 35.3 $\pm$ 2.4 nm, and after HCR, the size of MNP-SNAs increased to 123.6 $\pm$ 5.8 nm. These results can be explained by the formation of a long DNA biopolymer on the surface of MNPs. Figure 2B shows the fluorescence intensity of biotin-M3-carboxytetramethylrhodamine (TAMRA) directly conjugated to MNPs (M3-MNPs) (black curve) and self-assembled M3-TAMRA on the surface of MNPs after HCR (red curve). For the HCR, the fluorescence intensity showed an increase by a factor of about 5.0, indicating that high drug loading capacity could be realized by the number of AS1411 self-assembled on the surface of MNPs. The copies of M2 and M3 assembled on the surface of each MNP were quantified by fluorescence spectra, and the concentrations of biotin-labeled initiator, M2, and M3 are 101.7, 406.6, and 508.3 nM, respectively. In addition, in order to investigate the final structure of AS1411 embedded into the long DNA biopolymer on the surface of MNPs after HCR, H_2O_2, ABTS, and hemin were added to the constructed AS1411/MNP-SNAs. It is known that the complex of hemin/G-quadruplex can catalyze the H_2O_2-mediated oxidation of $ABTS^{2-}$ to the colored product $ABTS^{-}$.[38] From Figure S6, it was demonstrated that the initiator-conjugated MNP (black curve) had low absorbance at 418 nm in solution. After HCR, obvious enhanced absorbance changes (red curve) could be observed. These results confirmed the formation of the G-quadruplex structure of M3 on the surface of AS1411/MNP-SNAs.

Stability of AS1411/MNP-SNAs. Figure S7A shows the stability of the constructed AS1411/MNP-SNAs in fetal bovine serum (FBS) against degradation and digestion of DNase, as seen by the use of DLS. When the AS1411/MNP-SNAs were suspended in FBS and incubated for a series of time at 37 °C, the hydrodynamic size of AS1411/MNP-SNAs remained stable (from 0 to 8 h). Figure S7B also demonstrates the fluorescence intensity of TAMRA-labeled AS1411/MNP-SNAs as a function of incubation time with FBS at 37 °C. With an increase of the incubation time, a certain volume of AS1411/MNP-SNAs was collected to centrifuge for 15 min at 16 000 rpm, then the supernatant was discarded and resuspended in PBS buffer, and the fluorescence spectrum was recorded and no obvious fluorescence intensity change could be observed. These results showed that AS1411/MNP-SNAs were, indeed, efficient to provide protection against enzymatic cleavage and had the potential to be used for *in vivo* imaging and drug delivery.

Drug Loading of AS1411/MNP-SNAs. Since it is well-known that TMPyP4 can preferentially intercalate into the G-quadruplex, a red shift from 422 to 433 nm was carried out while the AS1411 was continually added to the TMPyP4 solution.[35] Therefore, if we fixed the excitation wavelength, addition of AS1411 would result in the quenching of drug fluorescence emission intensity. The drug loading experiment was performed by sequential addition of increasing fractions of AS1411/MNP-SNAs to TMPyP4 in PBS (the MNP itself cannot quench the fluorescence of TMPyP4; data not shown), and the fluorescence emission of the resultant solution was recorded. As shown in Figure 3A, the fluorescence of TMPyP4 (10 μM) was gradually quenched with increasing equivalences of AS1411/MNP-SNAs. When the fluorescence intensity was kept at the lowest point for 2 h at room temperature, the mixtures were centrifuged for 10 min at 12 000 rpm to remove the excess unloaded TMPyP4. Following collection of the

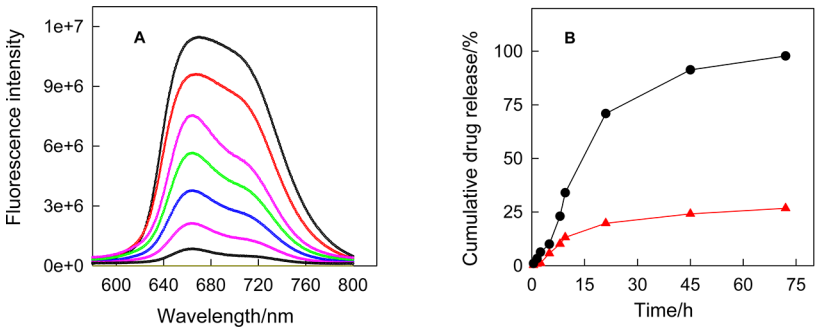

Figure 3. (A) Fluorescence spectra of TMPyP4 solution (10 μM) with increasing equivalences of AS1411/MNP-SNAs (from top to bottom: 0, 2.0, 5.0, 10, 15, 20, and 30 nM) with an excitation wavelength of 435 nm. (B) *In vitro* release profiles of free TMPyP4 (black line) and the AS1411/MNP-SNAs/TMPyP4 complex (red line).

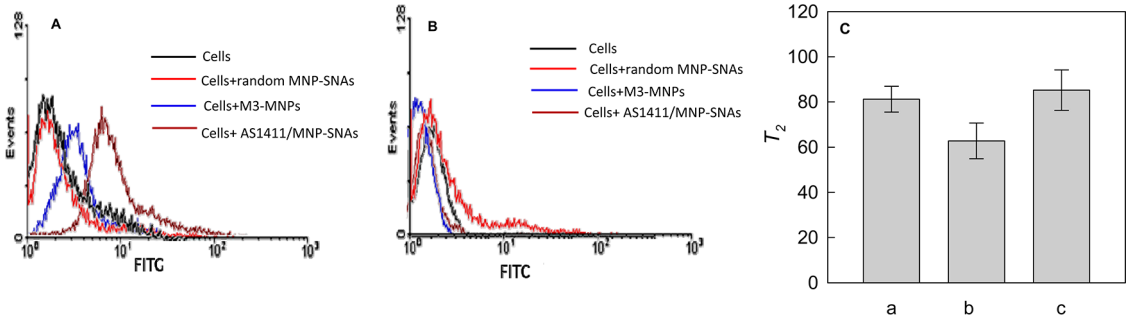

Figure 4. Binding study of AS1411/MNP-SNAs to different cells. (A,B) Flow cytometric assay to monitor the binding of FITC-labeled AS1411/MNP-SNAs to the target SKOV3 cells (A) and the control HBE135 cells (B) at 4 °C for 0.5 h. Cells, 200k/sample; AS1411-SNAs, 5.0 nM. (C) Spin–spin relaxation time (T_2) measurements of AS1411/MNP-SNAs (a), AS1411/MNP-SNAs incubated with SKOV3 cells (b), and HBE135 cells (c). The concentration of MNPs is 5.0 nM.

supernatants, the fluorescence intensity of the supernatants was tested. According to a standard curve of TMPyP4 (data not shown), we calculated that 98.5% TMPyP4 (9.85 μM) can be loaded into AS1411/MNP-SNAs. Similarly, M3-MNPs were also employed upon addition of the same amount as AS1411/MNP-SNAs, and about 17.8% TMPyP4 (the total concentration of TMPyP4 was also 10 μM) was loaded. From this result, we can conclude that high drug loading efficiency can be achieved for AS1411/MNP-SNAs. In addition, the rate of drug leakage from the AS1411/MNP-SNA carrier was slow since about one-sixth of the intercalated TMPyP4 dissociated in 21 h at 37 °C (Figure 3B). The slow leakage allowed sufficient time for the carrier–drug complex to target the cancer cells without losing any cargo and minimized possible side effects.

Specific Binding of AS1411/MNP-SNAs. To demonstrate the specific binding of AS1411 embedded in the biopolymer, random MNP-SNAs (constructed by carboxyfluorescein (FITC)-labeled M1 and M2, without AS1411) and AS1411/MNP-SNAs (constructed by FITC-labeled M1 and M3) were incubated with SKOV3 and HBE135 cells for 0.5 h, followed by flow cytometric analysis. A noticeable change in the fluorescence signal between random MNP-SNAs and AS1411/MNP-SNA-labeled SKOV3 cells indicated that the binding capability of the aptamer probes was maintained after conjugation with MNP-SNAs (Figure 4A). No significant change in fluorescence intensity was observed for HBE135 cells, a control cell line which did not bind with the AS1411 aptamer (Figure 4B), further confirming the specific recognition of the aptamer SNAs for target cells. It was noticed that the AS1411/MNP-SNA-targeted cells displayed enhanced fluorescence intensities compared to cells labeled with directly conjugated biotin-M3-FITC MNPs, essentially because one single AS1411/MNP-SNA can be loaded with multiple copies of fluorophores.

Using a benchtop nuclear magnetic resonance relaxometer, we further quantified the spin–spin relaxation times (T_2) of surrounding water protons in AS1411/MNP-SNAs only, AS1411/MNP-SNAs incubated with SKOV3 cells, and AS1411/MNP-SNAs incubated with HBE135 cells (Figure 4C). Aggregation of MNPs induces the coupling of magnetic spin moments and generates strong local magnetic fields. Such local magnetic field inhomogeneities accelerated the dephasing of adjacent water protons, resulting in a decrease of transverse or T_2.[39] Compared with AS1411/MNP-SNAs only, AS1411/MNP-SNAs treated with SKOV3 cells would induce effective cluster formation of AS1411/MNP-SNAs with SKOV3 cells because of the highly expressed nucleolin and thus show a huge decrease in the T_2 of the surrounding water protons, while AS1411/MNP-SNAs treated with HBE135 cells showed no obvious change. Overall, this evidence suggested that our

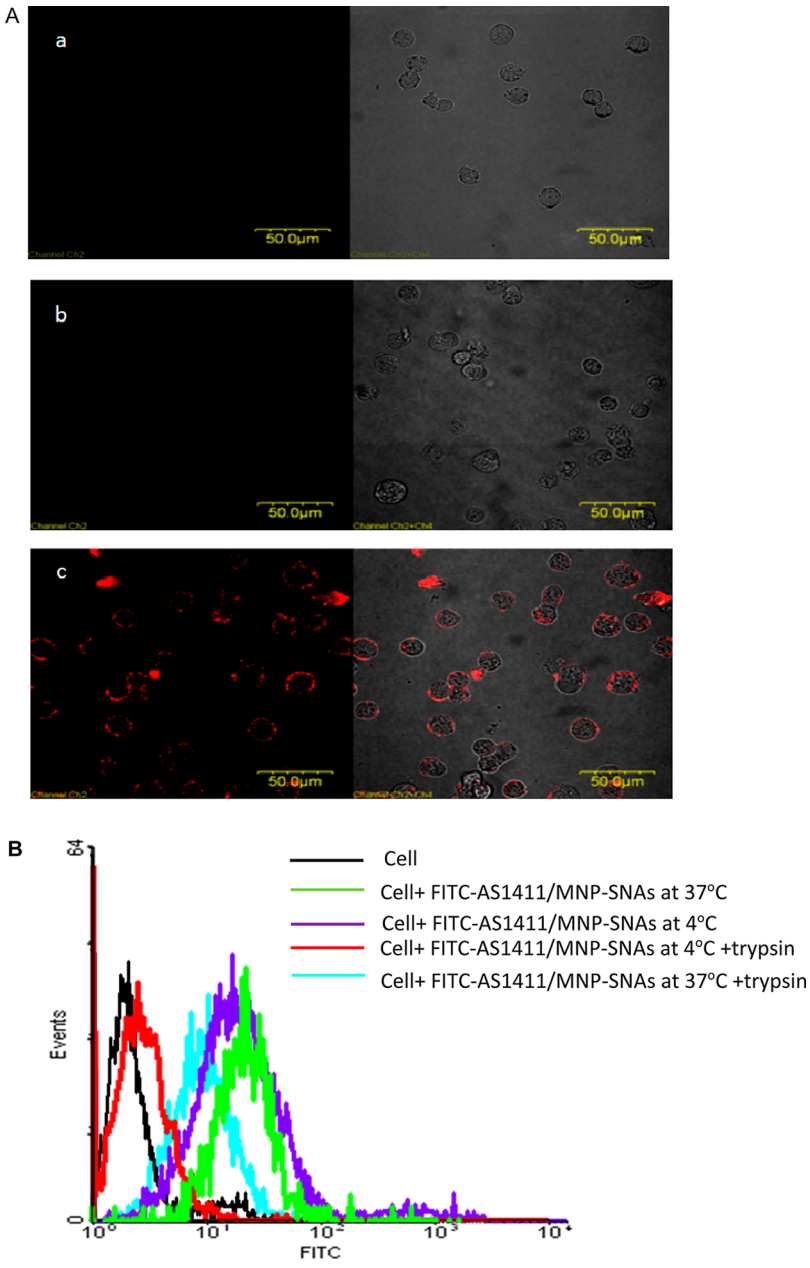

Figure 5. Internalization study of AS1411/MNP-SNAs to SKOV3 cells. (A) Confocal laser scanning microscopy images of SKOV3 cells (a), and the SKOV3 cells after treatments with random TAMAR-MNP-SNAs (b), and TAMRA-AS1411/MNP-SNAs (c) for 0.5 h. Left panels are TAMRA fluorescence pseudocolored red, and right panels are the overlay of TAMRA fluorescence and the bright-field image. (B) Flow cytometry results of FITC-AS1411/MNP-SNAs binding with SKOV3 under different conditions. The concentration of MNPs is 5 nM.

AS1411/MNP-SNA complexes are capable of specific recognition of target cancer cells.

Internalization of AS1411/MNP-SNAs. After 0.5 h incubation with TAMRA-labeled AS1411/MNP-SNAs, SKOV3 cells presented very bright fluorescence on their periphery under confocal microscopy imaging, whereas no fluorescence was displayed when using the TAMRA-labeled random MNP-SNAs at the same concentration (Figure 5A). We proceeded to characterize the internalization of the constructed AS1411/MNP-SNAs. The flow cytometry results in Figure 5B demonstrated that target SKOV3 cells showed a strong fluorescence signal at both 4 and 37 °C. The cells were then treated with trypsin at 37 °C to remove the external binding fluorescence signal that could interfere with the detection of the intracellular AS1411/MNP-SNAs.[40] In previous studies with aptamer Sgc8, our research group found that trypsin treatment is an easy method for this. Therefore, before flow cytometry and prior to the internalization study, trypsin was used to remove cell-surface-bound aptamers. After trypsin treatment, the fluorescence signal from flow cytometry of SKOV3 was very weak at 4 °C, but it still showed a high fluorescence signal at 37 °C, which can be attributed

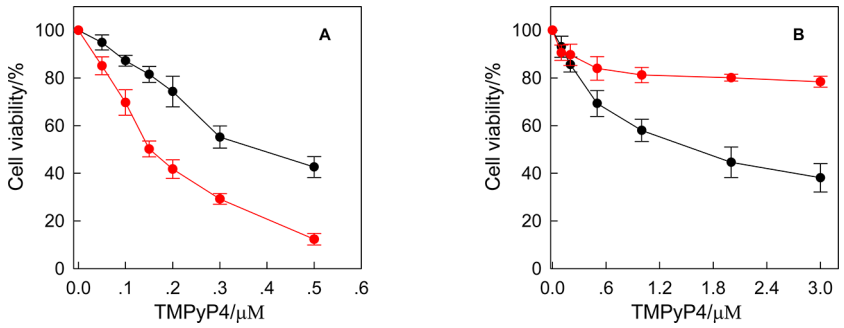

Figure 6. Cytotoxicity assay of (A) SKOV3 cells (target cells) and (B) HBE135 cells (control cells) treated with TMPyP4 only (black) and AS1411/MNP-SNA/TMPyP4 complex (red). The concentration of MNPs is 5 nM.

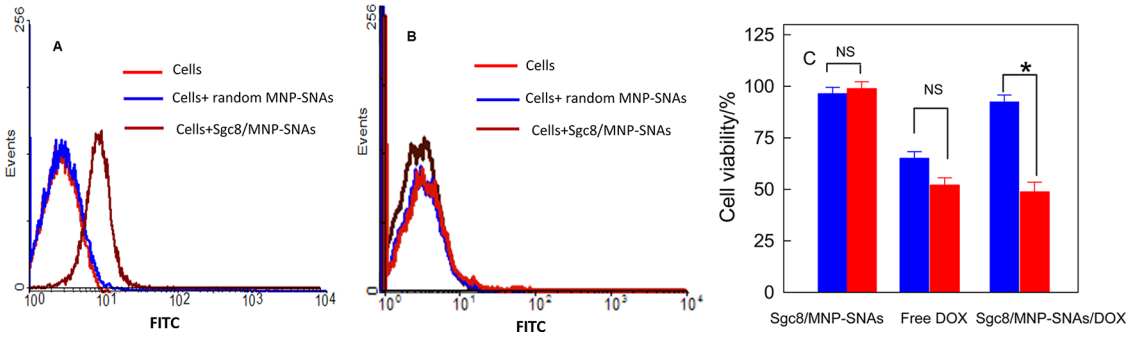

Figure 7. Flow cytometry results of Sgc8/MNP-SNAs binding with CEM (A) and Ramos (B) under different conditions. (C) Cell relative viability of CEM cells (red bar) and Ramos cells (blue bar) after treating with Sgc8/MNP-SNAs (left column), free DOX (middle column), and Sgc8/MNP-SNAs/DOX (right column). The DOX concentration is 0.5 μM. Each bar presents the mean and standard deviation derived from three independent experiments. *P* values were calculated by Student's test: ns, nonsignificance: $P > 0.30$ and * for $P < 0.02$, $n = 3$.

to the binding of aptamer to the cell membrane protein at 4 °C and the internalization at 37 °C, clearly demonstrating the internalization of AS1411/MNP-SNAs.

Cytotoxicity of the AS1411/MNP-SNA/TMPyP4 Complex. We next tested cell death induced by laser irradiation after AS1411/MNP-SNAs/TMPyP4, pure TMPyP4 labeling, and AS1411/MNP-SNAs. To accomplish this, cells were incubated with AS1411/MNP-SNAs/TMPyP4, pure TMPyP4, or AS1411/MNP-SNAs and then exposed to a laser light. Cell death was determined using propidium iodide (PI) dye to stain the dead cells, followed by flow cytometry monitoring. In AS1411/MNP-SNA-treated cells, no cytotoxicity could be observed (from 0 to 20 nM), even with light exposure (Figure S8). However, when the TMPyP4-treated or AS1411/MNP-SNA/TMPyP4-treated cells were irradiated with 1278 mJ cm^{-2} irradiation energy (180 s at 7.1 mW cm^{-2}), cell viability dramatically decreased. In comparing cell viability between SKOV3 and HBE135 after pure TMPyP4 drug treatment and then light exposure for 10 min (Figure 6), a higher phototoxicity in HBE135 cells than in SKOV3 cells was observed. However, the phototoxicity of the AS1411/MNP-SNA/TMPyP4 complex in SKOV3 was significantly higher than that in HBE135 cells after irradiation. These results demonstrated that the nucleolin-mediated uptake of MNP-SNAs, rather than nonspecific simple diffusion, significantly reduced the side effects of the TMPyP4 drug in normal epithelium cells and improved the degree of photodamage to cancer cells. These results further indicated that our aptamer-conjugated SNAs showed minimal nonspecific binding and were therefore highly promising for selective cell recognition and targeted cancer cell therapy.

Versatility of MNP-SNAs. Another advantage of this proposed multifunctional SNA platform is its general application for cancer therapy. To demonstrate, we constructed another self-assembled DNA polymer as the shell of these MNP-SNAs by capping the end of the DNA polymer with aptamer Sgc8, which can bind to target protein PTK7. PTK7 is overexpressed on the target CEM cell (CCL-119 T-cell, human acute lymphoblastic leukemia) surfaces but not on nontarget Ramos cells (CRL-1596, B-cell, human Burkitt's lymphoma).[41,42] After the construction of the SNAs, two FITC-labeled Sgc8 strands, I and II (see sequences in Table S1), were added to cap the end sequence and endow specific recognition capability (Figure S9 and Figure 7A,B). Doxorubicin (DOX), a chemotherapeutic drug, which is known to intercalate within the DNA strand by the presence of flat aromatic rings,[43] was loaded into these target-specific DNA MNP-SNAs (Figure S10). Having established that assembly of the DNA polymer can selectively recognize the target cells, the cytotoxic effect of Sgc8-MNP-SNAs/Dox was further evaluated

by using PI dye to stain the dead cells, followed by flow cytometry monitoring. Figure 7C demonstrates that unloaded Sgc8-MNP-SNAs had no effect on cell viability for either CEM or Ramos. In contrast, CEM cells, which had been labeled with Sgc8-MNP-SNAs/DOX and then incubated for 2 h, were killed with a percentage of 50.9%, while no effect could be observed for the Sgc8-MNP-SNA/DOX-labeled Ramos cells.

CONCLUSION

A new multifunctional SNA platform based on self-assembly of DNA polymer for cancer therapy was demonstrated in this paper. Compared with traditional SNAs, size controllability can be achieved by changing the length of the self-assembly DNA biopolymer shell, allowing, in turn, the potential to control cellular uptake, stability, biocompatibility, and surface functionalization. As proof of concept, a nucleolin-binding aptamer, AS1411, was self-assembled to prepare multifunctional SNAs. This complex combined imaging fluorescent tags, target recognition elements, and targeted delivery molecules into one conjugated acceptor, while possessing high drug loading and specificity. To demonstrate the generality of this multifunctional platform, aptamer-Sgc8 was capped on the end of the biopolymer to selectively deliver DOX to CEM cells. This approach might find potential applications in new drug development, existing drug improvement, and drug delivery for cancer therapy.

EXPERIMENT

Materials and Instruments. Doxorubicin (DOX) and 5,10,15,20-tetrakis(4-*N*-methylpyridiniumyl)porphyrin (TMPyP4) were purchased from Sigma Aldrich. AuNPs (13 nm) were synthesized according to a previous protocol.[28] Streptavidin-coated magnetic nanoparticles (MNPs, 30 nm) were purchased from Ocean Nanotech and dispersed at 0.1 mg/mL in 100 mM phosphate-buffered saline (PBS), pH 7.4. All chemicals were used as received, unless otherwise stated. The UV absorption titration was performed with a Cary 100 Bio UV/visible spectrophotometer (Varian, Inc.). The steady-state fluorescence measurements were recorded on a Fluorolog-Tau-3 spectrofluorometer (Jobin Yvon, Edison, NJ) with a 0.2 cm quartz cell using a band-pass of 5 nm for both excitation and emission. Dynamic light scattering (DLS) experiments were carried out in a Malvern Nano-ZS system equipped with a He−Ne laser working at 633 nm to examine the hydrodynamic diameter (number-weighted mean diameter).

DNA Synthesis. All DNA oligomers (see sequences in Table S1 in Supporting Information) were synthesized in our lab with an ABI3400 DNA/RNA synthesizer (Applied Biosystems, Foster City, CA, USA). DNA oligomers were deprotected in AMA (ammonium hydroxide/40% aqueous methylamine, 1:1) solution at 65 °C for 20−30 min and then transferred to 15 mL plastic tubes and mixed with 250 μL of 3.0 M NaCl and 6.0 mL of ethanol, followed by placement into a −20 °C freezer for precipitation. After centrifugation at 4000 rpm at 4 °C for 15−30 min, the precipitated DNA products were dissolved in 400 μL of 0.2 M triethylamine acetate (Glen Research Corp.) for HPLC purification with a C-18 reverse-phase HPLC column (ProStar, Varian, Walnut Creek, CA, USA). The collected DNA products were dried and detritylated by dissolving in 200 μL of 80% acetic acid for 20 min at room temperature and then precipitated with 20 μL of 3.0 M NaCl and 500 μL of ethanol at 20 °C, followed by drying with a vacuum dryer. Finally, the concentrations of DNA oligomers were measured with a Cary Bio-300 UV spectrometer (Varian, Walnut Creek, CA, USA). The characterizations of synthesized DNA were finished by Sangon, Shanghai, China. The representative ESI mass spectrum is shown in Figure S11.

Formation of SNAs Based on Self-Assembly of the DNA Biopolymer. For labeling AuNPs, 0.1 mM 5′-S−S-tagged initiator was incubated with 5 mM tris(2-carboxyethyl)phosphine (TCEP) in 50 mM Tris/HCl (pH 7.5) buffer for 1 h at room temperature to reduce S−S to SH groups. The 5′-SH initiator was then collected in small portions by eluting the TCEP mixture through a NAP-5 column. Then, a series of concentrations of initiator were reacted directly with the AuNPs through attachment of oligo-S-units onto the AuNP surfaces. After reaction for 24 h at room temperature, the mixtures were centrifuged for 25 min at 16 000 rpm to remove the excess thiol-DNA.[31] Following removal of the supernatants, the oily precipitates were washed with 4 mM trisodium citrate. After two wash/centrifuge cycles, the colloids were resuspended separately in 4 mM trisodium citrate and stored at 4 °C. For MNPs, biotin-labeled initiator sequences were first incubated with streptavidin-coated MNPs. The mixtures were vortexed at room temperature for 1 h followed by washing three times with PBS using centrifugation at 14 000 rpm to remove any DNA that did not conjugate to the MNPs. The conjugates were dispersed in PBS and stored at 4 °C at a concentration of 0.1 mg/mL.[39] Then, FITC-labeled M1 and M3 (see sequences in Table S1) were added to the solution containing initiator-conjugated nanoparticles, and the mixture was vortexed at room temperature for another 4 h followed by washing three times with PBS using centrifugation at 14 000 rpm to get the AS1411/MNP-SNAs. For the construction of random MNP-SNAs, FITC-labeled M1 and M2 (see sequences in Table S1) were added to the solution containing initiator-conjugated MNP, and the mixture was vortexed at room temperature for another 4 h followed by washing three times with PBS using centrifugation at 14 000 rpm to get the random MNP-SNAs.

Characterization of DNA Conjugated to the Nanoparticles. The conjugation of initiator on the AuNP surface was determined by absorption measurement. The absorption maxima (measured at 260 nm) of the supernatant, containing free initiator removed from the particle, were converted to molar concentrations of DNA by UV absorption using published sequence-dependent absorption coefficients. Finally, the average number of oligonucleotides per particle was obtained by dividing the measured oligonucleotide molar concentration by the original AuNP concentration. The conjugation of initiator on the MNPs' surface was determined by fluorescence measurement of fluorophore-labeled oligonucleotides. The fluorescence maxima of the supernatant, containing free initiator removed from the particle, were converted to molar concentrations of the fluorophore-modified oligonucleotide by interpolation from a standard linear calibration curve. Standard curves were prepared with known concentrations of fluorophore-labeled oligonucleotides using identical buffer pH and salt concentrations. The self-assembled M1, M2, and M3 on all sizes of SNAs were also determined using the same method (for M1, M2, and M3, they were labeled with different fluorophores).

AFM Imaging. AFM images were obtained by using a Nanoscope IIIa (Digital Instruments) operated under tapping mode. A drop of sample solution (5 μL) was spotted onto freshly cleaved mica (Ted Pella, Inc.) and left to adsorb to the surface for 30 s; then, 1× PBS buffer (50 μL) was placed onto the mica.

G-Quadruplex Formation of AS1411/MNP-SNAs. Low concentrations of AS1411/MNP-SNAs were suspended in PBS buffer, and ABTS/H_2O_2 substrate (1 and 2 mM, respectively) was added to the solution. The curves of absorbance at 420 nm *versus* wavelength were obtained using a Hitachi U-4100 UV/vis spectrophotometer (Kyoto, Japan).

Stability of AS1411/MNP-SNAs. The AS1411/MNP-SNAs were suspended in 3% FBS and incubated for a series of time at 37 °C (from 0 to 8 h), then the hydrodynamic size of AS1411/MNP-SNAs was characterized by the use of DLS. As for the fluorescence intensity detection, after incubation in 3% FBS for a series of time at 37 °C, 200 μL of AS1411/MNP-SNAs was removed and centrifuged for 15 min at 16 000 rpm; then the supernatant was discarded and resuspended in PBS buffer, and the fluorescence intensity was recorded on a Fluorolog-Tau-3 spectrofluorometer (Jobin Yvon, Edison, NJ).

Loading of TMPyP4. The formation of the AS1411/MNP-SNAs/TMPyP4 complex was monitored on the Fluorolog-Tau-3 spectrofluorometer. The TMPyP4 was diluted to 10 μM. The drug loading experiment was performed by sequential addition of increasing fractions of AS1411/MNP-SNAs to TMPyP4 in PBS buffer. When the fluorescence intensity was kept at the lowest point for 2 h at room temperature, the mixtures were centrifuged for 10 min at 12 000 rpm to remove the excess unloaded TMPyP4. Following collection of the supernatants, the fluorescence intensity of the supernatants was tested. According to a standard curve of TMPyP4, we calculated the loaded TMPyP4 into AS1411/MNP-SNAs.

Leakage of TMPyP4. To determine the leakage profile of TMPyP4 from the AS1411/MNP-SNAs, free TMPyP4 and the AS1411/MNP-SNAs/TMPyP4 complex in 200 μL of buffer were placed in Amicon Ultra-0.5 centrifugal filter devices with a cutoff of 30 kDa molecules. The centrifugal filter devices were soaked in 1.1 mL of buffer in the filtrate collection tubes and incubated at 37 °C. After 0.5, 1.5, 2.5, 5.0, 8.0, 9.5, 21, and 45 h, 120 μL of buffer was removed to measure TMPyP4 fluorescence using a FluoroMax-4 spectrofluorometer and then poured back into the filtrate collection tubes. After incubation for 21 h at 37 °C, the centrifugal devices were spun for 15 min at 14 000 rpm, and the fluorescence intensity of the filtrate was tested.

Binding of AS1411/MNP-SNAs with Cells. Human ovarian carcinoma cell line (SKOV3) and human normal bronchial epithelium cell line (HBE135) were washed with washing buffer and resuspended in binding buffer. Cells and AS1411/MNP-SNAs or random MNP-SNAs (both are labeled with FITC) were incubated on ice for 30 min. After washing with 1.0 mL of washing buffer, the cells were tested by a FACScan cytometer (Becton Dickinson Immunocytometry Systems, San Jose, CA, USA) by counting 20 000 events.

Relaxation Measurements. Spin−spin relaxation time (T_2) measurements were carried out at 1.4 T using a standard Carr Purcell Meiboom Gill Sequence on a benchtop Minispec mq60 TD-NMR contrast agent analyzer (Bruker Optics, Billerica, MA, USA). AS1411/MNP-SNAs only, AS1411/MNP-SNAs with SKOV3 cells, and AS1411/MNP-SNAs with HBE135 cells were incubated on ice for 30 min in 250 μL of PBS buffer in flow tubes. The final concentrations for AS1411/MNP-SNAs and cells were 5 nM and 10^6 cells/mL, respectively. To address AS1411/MNP-SNA aggregation and settling, samples were vortexed for more than 30 s. Then, all the samples were directly transferred into the NMR sample tubes and subjected to T_2 relaxation measurements without any further washing steps.

Internalization of AS1411/MNP-SNAs. First, cells were incubated with AS1411/MNP-SNAs or random MNP-SNAs (both are labeled with FITC) at 4 or 37 °C for 2 h. They were then washed with 1 mL of washing buffer to remove the unbound DNA sequences, then, incubated with trypsin (500 μL, 0.05%)/EDTA (0.53 mM) in HBSS at 37 °C for 10 min. After the incubation, the cells were washed twice with 1 mL of washing buffer and suspended in binding buffer (100 μL with 0.1% NaN_3) for the flow cytometric analysis and confocal imaging.

Cytotoxicity Test. Cell toxicity was tested by measuring the cell viability after treatment with AS1411/MNP-SNAs/TMPyP4 or TMPyP4 alone and irradiation using propidium iodide (PI) dye to stain the dead cells, followed by flow cytometry monitoring. Cells irradiated by the same lamp without drug treatment were considered to be 100% viable. In brief, SKOV3 and HBE135 cells were cultured at a density of 1×10^6 cells/mL in a 200 μL binding buffer at 37 °C for 2 h with a 5% CO_2 atmosphere, then washed twice with washing buffer. Then, they were irradiated for 10 min and returned to the incubator for another 48 h. Finally, cells were washed twice with 1 mL of PBS and incubated with trypsin (500 μL, 0.05%)/EDTA (0.53 mM) in HBSS at 37 °C for 10 min. Cells were scraped off the cell culture dish and stained with propidium iodide (Invitrogen, Carlsbad, CA, USA) at room temperature for 15 min to test cell viability. Dead cells, which can accumulate the dye and show red fluorescence, were determined by flow cytometric analysis.

Versatility of MNP-SNAs. For the construction of Sgc8/MNP-SNAs, biotin-labeled initiator sequences were first incubated with streptavidin-coated MNPs. The mixtures were vortexed at room temperature for 1 h followed by washing three times with PBS using centrifugation at 14 000 rpm to remove any DNA that did not conjugate to the MNPs. The conjugates were dispersed in PBS and stored at 4 °C at a concentration of 0.1 mg/mL.[39] Then, M2 and M3 (see sequences in Table S1) were added to the solution containing initiator-conjugated nanoparticles, and the mixture was vortexed at room temperature for another 4 h followed by washing three times with PBS using centrifugation at 14 000 rpm. At last, the Sgc8 capped-strand I/II-FITC was added to the mixture and vortexed at room temperature for 2 h followed by washing three times with PBS using centrifugation at 14 000 rpm. As for the drug loading, target-cell-specific binding, and cytotoxicity test, the procedures were the same as the AS1411/MNP-SNAs.

Conflict of Interest: The authors declare no competing financial interest.

Acknowledgment. We appreciate Dr. Kathryn Williams for her help with manuscript preparation and revision, and Mr. Cuichen Sam Wu for his helpful discussion. J.Z. received a scholarship award for Excellent Doctoral Student granted by the Ministry of Education, China. This work is supported by grants awarded by the National Key Scientific Program of China (2011CB911000), the Foundation for Innovative Research Groups of NSFC (Grant 21221003), NSFC (21005026 and 21135001), China National Instrumentation Program 2011YQ03012412 and China National Grand Program (2009ZX10004-312). It is also supported by the National Institutes of Health (GM079359 and CA133086).

Supporting Information Available: Details of DNA sequences used in this experiment; absorption spectra and TEM images of AuNPs; agarose gel electrophoresis images of DNA biopolymer; TMPyP4 loading; DOX loading; cytotoxicity assay of AS1411/MNP-SNAs; Sgc8 aptamer-capped MNP-SNA characterization. This material is available free of charge *via* the Internet at http://pubs.acs.org.

REFERENCES AND NOTES

1. Lin, C.; Liu, Y.; Yan, H. Designer DNA Nanoarchitectures. *Biochemistry* **2009**, *48*, 1663–1674.
2. Douglas, S. M.; Dietz, H.; Liedl, T.; Hogberg, B.; Graf, F.; Shih, W. M. Self-Assembly of DNA into Nanoscale Three-Dimensional Shapes. *Nature* **2009**, *459*, 414–418.
3. Seeman, N. C. J. Design of Immobile Nucleic Acid Junctions. *Theor. Biol.* **1982**, *99*, 237–247.
4. Pei, H.; Liang, L.; Yao, G. B.; Li, J.; Huang, Q.; Fan, C. H. Reconfigurable Three-Dimensional DNA Nanostructures for the Construction of Intracellular Logic Sensors. *Angew. Chem., Int. Ed.* **2012**, *51*, 9020–9024.
5. Hayriye, O.; Bruce, A. A. Fluorescent DNA Nanotags Based on a Self-Assembled DNA Tetrahedron. *ACS Nano* **2009**, *3*, 425–433.
6. Yurke, B.; Turberfield, A. J.; Mills, A., Jr.; Simmel, F. C.; Neumann, J. L. A DNA-Fuelled Molecular Machine Made of DNA. *Nature* **2000**, *406*, 605–608.
7. Liu, C. H.; Jonoska, N.; Seeman, N. C. Reciprocal DNA Nanomechanical Devices Controlled by the Same Set Strands. *Nano Lett.* **2009**, *9*, 2641–2647.
8. Thomas, J. M.; Yu, H. Z.; Sen, D. A Mechano-Electronic DNA Switch. *J. Am. Chem. Soc.* **2012**, *134*, 13738–13748.
9. Nishikawa, M.; Mizuno, Y.; Mohri, K.; Matsuoka, N.; Rattanakiat, S.; Takahashi, Y.; Funabashi, H.; Luo, D.; Takakura, Y. Biodegradable CpG DNA Hydrogels for Sustained Delivery

of Doxorubicin and Immunostimulatory Signals in Tumor-Bearing Mice. *Biomaterials* **2011**, *32*, 488–494.
10. Jiang, Q.; Song, C.; Nangreave, J.; Liu, X. W.; Lin, L.; Yan, H.; Ding, B. Q. DNA Origami as a Carrier for Circumvention of Drug Resistance. *J. Am. Chem. Soc.* **2012**, *134*, 13396–13403.
11. Mirkin, C. A.; Letsinger, R. L.; Mucic, R. C.; Storhoff, J. J. A DNA-Based Method for Rationally Assembling Nanoparticles into Macroscopic Materials. *Nature* **1996**, *382*, 607–609.
12. Farokhzad, O. C.; Langer, R. Nanomedicine: Developing Smarter Therapeutic and Diagnostic Modalities. *Adv. Drug Delivery Rev.* **2006**, *58*, 1456–1459.
13. Rosi, N. L.; Mirkin, C. A. Nanostructures in Biodiagnostics. *Chem. Rev.* **2005**, *105*, 1547–1562.
14. Weiss, S.; Bruchez, M.; Moronne, M.; Gin, P.; Alivisatos, A. P. Semiconductor Nanocrystals as Fluorescent Biological Labels. *Science* **1998**, *281*, 2013–2016.
15. Verma, A.; Simard, J. M.; Worrall, J. W.; Rotello, V. M. Tunable Reactivation of Nanoparticle-Inhibited β-Galactosidase by Glutathione at Intracellular Concentrations. *J. Am. Chem. Soc.* **2004**, *126*, 13987–13991.
16. Seferos, D. S.; Giljohann, D. A.; Hill, H. D.; Prigodich, A. E.; Mirkin, C. A. Nano-Flares: Probes for Transfection and mRNA Detection in Living Cells. *J. Am. Chem. Soc.* **2007**, *129*, 15477–15479.
17. Giljohann, D. A.; Seferos, D. S.; Daniel, W. L.; Massich, M. D.; Patel, P. C.; Mirkin, C. A. Gold Nanoparticles for Biology and Medicine. *Angew. Chem., Int. Ed.* **2010**, *49*, 3280–3294.
18. Rosi, N. L.; Giljohann, D. A.; Thaxton, C. S.; Lytton-Jean, A. K. R.; Han, M. S.; Mirkin, C. A. Oligonucleotide-Modified Gold Nanoparticles for Intracellular Gene Regulation. *Science* **2006**, *312*, 1027–1030.
19. Maltzahn, V. G.; Park, J. H.; Lin, K. Y.; Singh, N.; Schwoppe, C.; Mesters, R.; Berdel, W. E.; Ruoslahti, E.; Sailor, M. J.; Bhatia, S. N. Nanoparticles That Communicate *in Vivo* To Amplify Tumour Targeting. *Nat. Mater.* **2011**, *10*, 545–552.
20. Giljohann, D. A.; Seferos, D. S.; Prigodich, A. E.; Patel, P. C.; Mirkin, C. A. Gene Regulation with Polyvalent siRNA-Nanoparticle Conjugates. *J. Am. Chem. Soc.* **2009**, *131*, 2072–2073.
21. Davis, M. E.; Chen, Z.; Shin, D. M. Nanoparticle Therapeutics: An Emerging Treatment Modality for Cancer. *Nat. Rev. Drug Discovery* **2008**, *7*, 771–782.
22. Dobson, J. Gene Therapy Progress and Prospects: Magnetic Nanoparticle-Based Gene Delivery. *Gene Ther.* **2006**, *13*, 283–287.
23. Zhang, X. Q.; Xu, X. Y.; Lam, R.; Giljohann, D.; Ho, D.; Mirkin, C. A. Strategy for Increasing Drug Solubility and Efficacy through Covalent Attachment to Polyvalent DNA-Nanoparticle Conjugates. *ACS Nano* **2011**, *5*, 6962–6970.
24. Jiang, W.; Kim, B. Y. S.; Rutka, J. T.; Chan, W. C. W. Nanoparticle-Mediated Cellular Response is Size-Dependent. *Nat. Nanotechnol.* **2008**, *3*, 145–150.
25. Oh, W. K.; Kim, S.; Choi, M.; Kim, C.; Jeong, Y. S.; Cho, B. R.; Hahn, J. S.; Jiang, S. Cellular Uptake, Cytotoxicity, and Innate Immune Response of Silica Titania Hollow Nanoparticles Based on Size and Surface Functionality. *ACS Nano* **2010**, *4*, 5301–5313.
26. Colombo, M.; Romero, S. C.; Casula, M. F.; Gutierrez, L.; Morales, M. P.; Bohm, I. B.; Heverhagen, J. T.; Prosperi, D.; Parak, W. J. Biological Applications of Magnetic Nanoparticles. *Chem. Soc. Rev.* **2012**, *41*, 4306–4334.
27. Dirks, R. M.; Pierce, N. A. Triggered Amplification by Hybridization Chain Reaction. *Proc. Natl. Acad. Sci. U.S.A.* **2004**, *101*, 15275–15278.
28. Liu, J. W.; Lu, Y. Preparation of Aptamer-Linked Gold Nanoparticle Purple Aggregates for Colorimetric Sensing of Analytes. *Nat. Protoc.* **2006**, *1*, 246–252.
29. Kelley, A. T.; Alessi, P. J.; Fornalik, J. E.; Minter, J. R.; Royster, T. L. Investigation and Application of Nanoparticle Dispersions of Pigment Yellow 185 Using Organic Solvents. *ACS Appl. Mater. Interfaces* **2010**, *2*, 61–68.
30. Hwang, D. W.; Ko, H. Y.; Lee, J. H.; Kang, H.; Ryu, S. H.; Song, I. C. A Nucleolin-Targeted Multimodal Nanoparticle Imaging Probe for Tracking Cancer Cells Using an Aptamer. *J. Nucl. Med.* **2010**, *51*, e105.
31. Wei, C.; Jia, G.; Yuan, J.; Feng, Z.; Li, C. A Spectroscopic Study on the Interactions of Porphyrin with G-Quadruplex DNAs. *Biochemistry* **2006**, *45*, 6681–6691.
32. Martino, L.; Pagano, B.; Fotticchia, I.; Neidle, S.; Giancola, C. A New Cationic Porphyrin Derivative (TMPipEOPP) with Large Side Arm Substituents: A Highly Selective G-Quadruplex Optical Probe. *PloS One* **2012**, *7*, e35586.
33. Wang, K. L.; You, M. X.; Chen, Y.; Han, D.; Zhu, Z.; Huang, J.; Williams, K.; Yang, C. J.; Tan, W. H. Self-Assembly of a Bifunctional DNA Carrier for Drug Delivery. *Angew. Chem., Int. Ed.* **2011**, *50*, 6098–6101.
34. Zhang, H.; Wang, X.; Wang, P.; Pang, S.; Ai, X.; Zhang, J. Interactions between *meso*-Tetrakis(4-(*N*-methylpyridiumyl)) Porphyrin TMPyP4 and DNA G-Quadruplex of Telomeric Repeated Sequence TTAGGG. *Sci. China, Ser. B* **2008**, *51*, 452–456.
35. Rha, S. Y.; Izbicka, E.; Lawrence, R.; Davidson, K.; Sun, D.; Moyer, M. P.; Roodman, G. D.; Hurley, L.; Von Hoff, D. Effect of Telomere and Telomerase Interactive Agents on Human Tumor and Normal Cell Lines. *Clin. Cancer Res.* **2000**, *6*, 987–993.
36. Shieh, Y. A.; Yang, S. J.; Wei, M. F.; Shieh, M. J. Aptamer-Based Tumor-Targeted Drug Delivery for Photodynamic Therapy. *ACS Nano* **2010**, *4*, 1433–1442.
37. Yin, M. L.; Li, Z. H.; Liu, Z.; Ren, J. S.; Yang, X. J.; Qu, X. G. Photosensitizer-Incorporated G-Quadruplex DNA-Functionalized Magnetic Resonance/Fluorescence Nanoparticles for Targeted Magnetic Resonance/Fluorescence Multimodal Imaging and Subsequent Photodynamic Therapy of Cancer. *Chem. Commun.* **2012**, *48*, 6556–6558.
38. Travascio, P.; Li, Y.; Sen, D. DNA-Enhanced Peroxidase Activity of a DNA Aptamer-Hemin Complex. *Chem. Biol.* **1998**, *5*, 505–517.
39. Bamrungsap, S.; Chen, T.; Shukoor, M. I.; Chen, Z.; Sefah, K.; Chen, Y.; Tan, W. H. Pattern Recognition of Cancer Cells Using Aptamer-Conjugated Magnetic Nanoparticles. *ACS Nano* **2012**, *6*, 3974–3981.
40. Xiao, Z.; Shangguan, D.; Cao, Z.; Fang, X.; Tan, W. Cell-Specific Internalization Study of an Aptamer from Whole Cell Selection. *Chem.—Eur. J.* **2008**, *14*, 1769–1775.
41. Shangguan, D. H.; Li, Y.; Tang, Z. W.; Cao, Z. H.; Chen, H. W.; Mallikaratchy, P.; Sefah, K.; Yang, C. J.; Tan, W. H. Aptamers Evolved from Live Cells as Effective Molecular Probes for Cancer Study. *Proc. Natl. Acad. Sci. U.S.A.* **2006**, *103*, 11838–11843.
42. Shangguan, D.; Cao, Z.; Meng, L.; Mallikaratchy, P.; Sefah, K.; Wang, H.; Li, Y.; Tan, W. H. Cell-Specific Aptamer Probes for Membrane Protein Elucidation in Cancer Cells. *J. Proteome Res.* **2008**, *7*, 2133–2139.
43. Zhu, G. Z.; Meng, L.; Yang, L.; Tan, W. H. Self-Assembled Aptamer-Based Drug Carriers for Bispecific Cytotoxicity to Cancer Cells. *Chem.—Asian . J.* **2012**, *7*, 1630–1636.